

Article

An Efficient Dopant for Introducing Magnetism into Topological Insulator Bi_2Se_3

Dan Wang ¹, Cui-E Hu ², Li-Gang Liu ³, Min Zhang ^{3,*} and Xiang-Rong Chen ^{1,*} ¹ Institute of Atomic and Molecular Physics, Sichuan University, Chengdu 610065, China; wangdankr@163.com² College of Physics and Electronic Engineering, Chongqing Normal University, Chongqing 400047, China; cuiehu@126.com³ School of Physics and Astronomy, China West Normal University, Nanchong 637002, China; llg218@126.com

* Correspondence: zmzmi1987@163.com (M.Z.); xrchen@scu.edu.cn (X.-R.C.)

Abstract: In this work, we obtained an effective way to introduce magnetism into topological insulators, and successfully fabricated single crystal C- Bi_2Se_3 . The structural, electrical and magnetic properties of non-magnetic element X (B, C and N) doped at Bi, Se1, Se2 and VDW gap sites of Bi_2Se_3 were studied by the first principles. It is shown that the impurity bands formed inside the bulk inverted energy gap near the Fermi level with C doping Bi_2Se_3 . Due to spin-polarized ferromagnetic coupling, the time inversion symmetry of Bi_2Se_3 is destroyed. Remarkably, C is the most effective dopant because of the magnetic moment produced by doping at all positions. The experiment confirmed that the remnant ferromagnetism M_r is related to the C concentration. Theoretical calculations and experiments confirmed that carbon-doped Bi_2Se_3 is ferromagnetic, which provides a plan for manipulating topological properties and exploring spintronic applications.

Keywords: topological insulator; Bi_2Se_3 ; density functional theory; magnetism



Citation: Wang, D.; Hu, C.-E.; Liu, L.-G.; Zhang, M.; Chen, X.-R. An Efficient Dopant for Introducing Magnetism into Topological Insulator Bi_2Se_3 . *Materials* **2022**, *15*, 3864. <https://doi.org/10.3390/ma15113864>

Academic Editor: Simone Pisana

Received: 19 April 2022

Accepted: 25 May 2022

Published: 28 May 2022

Publisher's Note: MDPI stays neutral with regard to jurisdictional claims in published maps and institutional affiliations.



Copyright: © 2022 by the authors. Licensee MDPI, Basel, Switzerland. This article is an open access article distributed under the terms and conditions of the Creative Commons Attribution (CC BY) license (<https://creativecommons.org/licenses/by/4.0/>).

1. Introduction

Bi_2Se_3 is a famous three-dimensional (3D) topological insulator (TI) with large bulk band gap and metallic helical states on the surface [1]. The gapless surface states with single Dirac electrons are defended by the time-reversal symmetry and are robust against crystal defects and non-magnetic impurities [2–6]. The interaction between topological properties and magnetism destroys time-reversal symmetry in the presence of band hybridizations [7–9]. The quantized anomalous Hall effect (QAHE), magneto-optical effect, magnetic monopole and Majorana fermion have been demonstrated in magnetic topological insulators [7,10–12]. To date, the magnetic introduction of Bi_2Se_3 has mainly been focused on the magnetic proximity effect [13] and transition metals doping [14].

It is shown that the exchange coupling of magnetic materials can produce a proximity effect and induce magnetism in topological insulators [15,16]. However, magnetic materials are required to be insulating materials with poor conductivity and ferromagnetism. In terms of preparation, the crystal structure of the material is matched with that of Bi_2Se_3 , avoiding the occurrence of impurities and defect states. Experimentally, the proximity-induced interfacial magnetization of Bi_2Se_3 has been realized in the systems with FeSe_2 [17], EuS [18], Cr_2O_3 [19], MnSe [20], LaCoO_3 [21], $\text{Ni}_{80}\text{Fe}_{20}$ [22], SiO_2 [23].

The magnetic elements doping can tune the bandgap and produce magnetism. Bi_2Se_3 thin films with Cr doping present a magnetic ground state with ferromagnetic planes coupled antiferromagnetically [24,25] and opened the band gap at the Dirac point [26]. The films of Cr and Sb doping Bi_2Se_3 exhibited enhanced weak localization-like positive magneto conductivity and ferromagnetism [27]. According to the literature, Mn-doped Bi_2Se_3 showed a spin glass state, paramagnetic state and ferromagnetism [28–33]. A ferromagnetic-paramagnetic transition with increasing Mn concentration was observed [34]. Li [35] reported that the ferromagnetism in Bi_2Se_3 with Fe doping is not intrinsic. Fe- and Ni-doped

Bi_2Se_3 samples showed diamagnetism, paramagnetism and ferromagnetism with different doping concentrations [36–39], and the surface of the samples formed a small amount of ferromagnet compounds. Obvious ferromagnetism was observed in Co-doped Bi_2Se_3 [40,41]. In addition, it was found that other metal elements such as rare earth elements (Dy, Ho, Eu, Gd) and alkaline earth elements (Sr, Ca) can also introduce magnetism [42–50]. However, the weaknesses of magnetic atoms doping are that clusters or secondary phases will be formed during the crystal growth and the source of the magnetism is unclear.

Thus, it is beneficial to obtain magnetic ordering in non-magnetic materials without transition metal or rare-earth species, which can avoid producing magnetic second phases. As we all know, the magnetism is originated from the presence of highly localized unpaired electrons in 3d and 4f orbitals of the transition and rare-earth metals. Interestingly, the 2p electrons of the light elements B, N and C have similar properties to 3d states of transition metals [51,52]. It has been reported that non-magnetic 2p light element-doped semiconductors can produce d^0 ferromagnetism [53]. Different from the traditional magnetic semiconductors, the cluster structure formed by the doped elements has no contribution to the magnetic order of the system. Brahmananda predicted the room temperature ferromagnetism (FM) in C-doped Y_2O_3 [54] and MoO_3 [55]. Niu [13] demonstrated that Bi_2Se_3 with B, C and N doping is ferromagnetic. The doping is mostly concentrated at the Se site, and it is not considered that the doping elements may replace the Bi site or appear in the VDW gap. Xin et al. [56] studied the C element doping at the Se site and gap of Bi_2Se_3 and found that the system is spin-polarized. The first-principles study indicated that C doping can introduce a magnetic moment. They mainly focused on the gap sites and explained the cause of magnetism. One widely discussed scenario for introducing magnetism in non-magnetic materials involves the substitutional doping of C impurities. There are few detailed identifications for other 2p light elements-doped TI. Thus, we systematically calculated the structural and magnetic properties of the X (B, C and N) atoms doping at Bi, Se and gap sites of Bi_2Se_3 to further understand the details of 2p light element doping Bi_2Se_3 and effectively introduce magnetism into topological insulators. Our theoretical results reveal that C is the most effective dopant because of the magnetic moment produced by doping at all positions. Meanwhile, C-doped topological insulator crystals were grown and their magnetic properties were studied. These single crystals are ferromagnetic with small magnetic moments, and the remnant ferromagnetism M_r is related to the C concentration. It is possible to introduce magnetism by non-magnetic doping and find a system that can realize peculiar physical effects such as the quantum anomalous Hall effect (QAHE).

2. Experimental and Computational Details

2.1. Preparation and Characterization of Single Crystal Bi_2Se_3

The single crystalline $\text{C}_x\text{Bi}_2\text{Se}_3$ ($x = 0, 0.02, 0.04, 0.06$) was prepared from the reactions of the stoichiometric mixture of carbon (99.99%), Bi (99.999%) and Se (99.999%) powders. The mixed powders were placed in quartz ampoule that was sealed in vacuum with a pressure of 10^{-5} Pa. The quartz ampoule was put into a resistance furnace which was heated at 1170 K for 24 h. Then, it was cooled slowly to and kept at 920 K for 3 days. Finally, it was quenched in cold water. The single crystal was well cleavable. Magnetic measurements were performed using a superconducting quantum-interference device (SQUID, Quantum Design) magnetometer. Field emission scanning electron microscopy (FE-SEM, JSM-7001F) was used to detect the morphology of the samples.

2.2. Theoretical Method and Computational Details

The calculations were performed within density functional theory using the Vienna ab initio simulation package (VASP) [57]. The PBE [58] generalized gradient approximation and the projector augmented wave potentials [59] were employed to describe the exchange-correlation functional and the core-electron interaction, respectively. The cut-off energy of all the systems based on the plane wave expansion was set to 500 eV. The integration over the Brillouin zone was done using the Monkhorst–Pack mesh of $3 \times 3 \times 1$. All structures

were fully optimized until the convergent threshold for energy was 10^{-5} eV/atom and the Hellmann–Feynman force acting on each atom was 0.01 eV/nm $^{-1}$. The valence electron configuration of each atom was: B $2s^22p^1$, C $2s^22p^2$, N $2s^22p^3$, Se $4s^24p^4$, Bi $6s^26p^3$. The structure relaxation with DFT-D2 and self-consistent with the spin-orbit coupling (SOC) was calculated.

3. Results and Discussions

3.1. Geometrical Structure and Magnetic Properties of X Doping Bi₂Se₃

The crystal structure of Bi₂Se₃ is rhombohedral, belonging to the space group D_{3d}^5 ($R\bar{3}m$) [60]. As show in Figure 1a, the rhombohedral unit cell contains three Se atoms and two Bi atoms. The hexagonal unit cell has three sets of quintuple layers (QL) with five atomic layers in Figure 1b. The five layers form a stable unit in the order of Se1-Bi-Se2-Bi-Se1 with strong covalent bonds, while the inter-layer bonding is much weaker because of the van der Waals forces. These nonequivalent Se atoms are denoted as Se1 and Se2. The Se2 atom surrounded by Bi atoms is the spatial inversion symmetry center. To study the results of X doping different configurations in Bi₂Se₃, we considered the following cases: the Bi site, the non-equivalent Se1 and Se2 sites and the VDW gap site in the $2 \times 2 \times 1$ supercell containing 36 Se atoms and 24 Bi atoms, labeled XBi, XSe1, XSe2 and Xgap. Figure 1c–f are the optimized structure diagrams of Bi₂₃Se₃₆XBi, Bi₂₄Se₃₅XSe1, Bi₂₄Se₃₅XSe2 and Bi₂₄Se₃₆Xgap, respectively. The change of structure is not particularly obvious with the small doping proportions. The X atom moves close to the Bi and Se1 atoms and forms the X-Se1, X-Bi covalent bond. In Table 1, the strength of covalent bonding increasing accompanies the reducing of the bond length between dopant X and nearby atoms. The bond lengths in the primitive cell are: Se1-Bi, 2.865 Å; Se2-Bi, 3.067 Å and Se1-Se2, 4.36 Å. However, the structure still maintains a high symmetry because the impact on the other QL is inconspicuous.

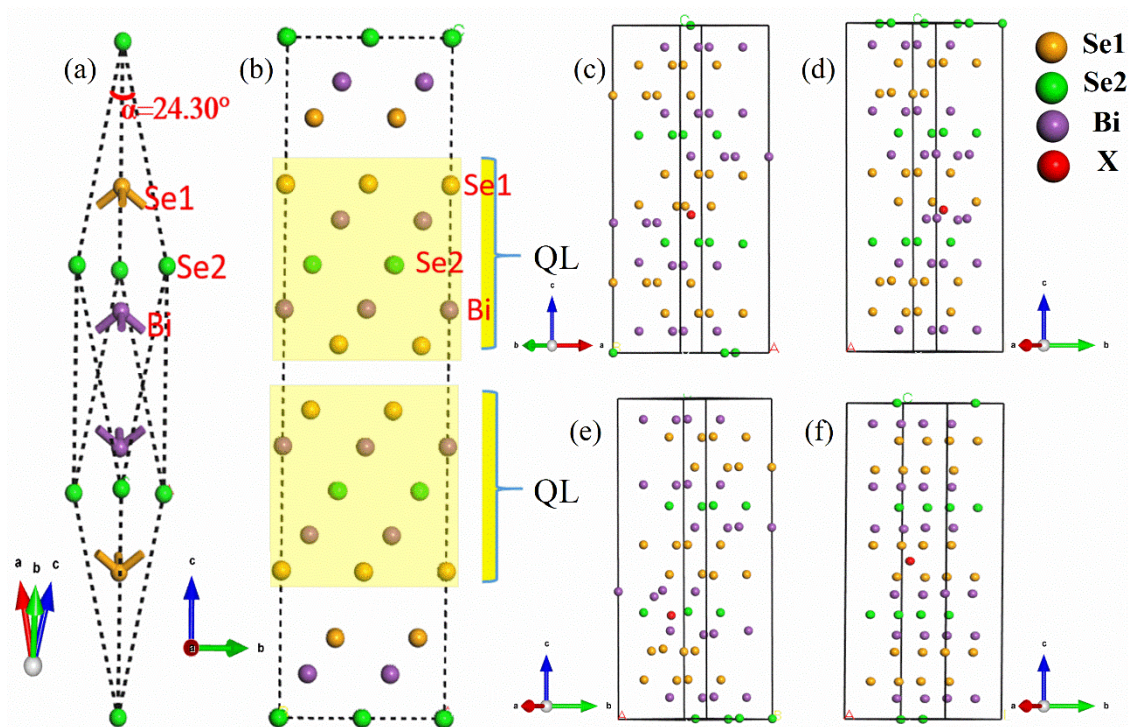


Figure 1. (a) The rhombohedral unit cell of Bi₂Se₃, (b) 60-atom layered crystal structure of Bi₂Se₃, (c) structure of Bi₂₃Se₃₆XBi, (d) structure of Bi₂₄Se₃₅XSe1, (e) structure of Bi₂₄Se₃₅XSe2, and (f) structure of Bi₂₄Se₃₆Xgap.

Table 1. Formation energies, bond lengths and magnetic moments of X doping Bi₂Se₃.

	E_{from} (eV)	$d_{\text{X-Bi}}$ (Å)	$d_{\text{X-Se}}$ (Å)	M_{tot} (μB)	M_{X} (μB)	M_{tot} (μB) _{·exp}
BBi	−4.565	/	1.979	0.978	0.208	
BSe1	−11.007	2.460	/	0	0	0.44 ^a
BSe2	−10.52	2.838	/	1.416	0.413	3.0 ^a
Bgap	−12.177	/	1.832	0	0	
CBi	−0.808	/	1.885	0.410	0.164	
CSe1	−9.933	2.369	/	0.649	0.377	2.0 ^a , 1.66 ^b
CSe2	−9.492	2.798	/	0.980	0.375	2.0 ^a , 1.95 ^b
Cgap	−9.975	/	1.801	0.673	0.225	1.53 ^b
NBi	−16.216	/	1.997	0	0	
NSe1	−17.418	2.285	/	0	0	0.14 ^a
NSe2	−17.151	2.325	/	0.094	0.028	1.0 ^a
Ngap	−16.303	/	1.956	0.794	0.576	

^a Data taken from Ref. [13]. ^b Data taken from Ref. [56].

The formation energy of Bi₂Se₃ is given by $E_{\text{Bi}_2\text{Se}_3} = E_{\text{pure}} - (36 E_{\text{Se}} + 24 E_{\text{Bi}}) = -31.362$ eV. The formation energy is relevant to the relative stability of structures. Through X doping, the formation energy is computed using the following formulas:

$$E_{\text{XBi}} = E_{\text{doped}} - E_{\text{pure}} - E_{\text{X}} + E_{\text{Bi}} \quad (1)$$

$$E_{\text{XSe}} = E_{\text{doped}} - E_{\text{pure}} - E_{\text{X}} + E_{\text{Se}} \quad (2)$$

$$E_{\text{Xgap}} = E_{\text{doped}} - E_{\text{pure}} - E_{\text{X}} \quad (3)$$

where E_{XBi} is the formation energies of the X atom-doped Bi site; E_{XSe} is the formation energies of the X atom-doped Se1, Se2 site; E_{Xgap} represents the formation energies of the X atom-doped gap site; E_{doped} and E_{pure} are the total energies of the X-doped and pure Bi₂Se₃; and E_{X} , E_{Bi} and E_{Se} are the energies of the X, Bi and Se atom, respectively. The negative energies mean that X atom-doped Bi₂Se₃ can be realized experimentally. As shown in Table 1, the formation energies of the structures with B, C doping at the gap site are lower than those of the structures with substitution at various sites. It is reasonable that those configurations gain large bonding energy due to the strong chemical bonding and then cause a drop in formation energy in these systems. Theoretically, the N atoms with a smaller covalent radius (0.741 Å) (B: 0.905 Å, C: 0.863 Å) are energetically favorable as dopants in Bi₂Se₃. The Bi₂₄Se₃₅NSe1 structure is the most energetically favorable, because the N atom with more free electrons can more easily bond with a Bi atom (bond length: N-Bi: 2.285 Å). In general, the B, C doping gap site and N doping Se1 sites are the most energetically favorable. The X atoms replacing Bi atoms are found to be energetically unfavorable as dopants in Bi₂Se₃.

The magnetic properties are calculated because the unpaired electrons are introduced with X atom doping. The ferromagnetic (E_{FM}) and antiferromagnetic (E_{AFM}) energies with four doped X atoms are calculated to judge the magnetic static state. The E_{FM} and E_{AFM} in Bi₂₄Se₃₂X₄ are −248.801 eV and −248.786 eV, −276.604 eV and −273.49 eV, −254.697 eV and −254.521 eV, respectively. This demonstrates that the ferromagnetic interaction is more favorable than the antiferromagnetic one, and the system of X doping Bi₂Se₃ is ferromagnetic. Xin [56] reported the single crystal Bi₂C_xSe_{3−x} ($x = 0.05$) sample is a FM state which excludes magnetic impurities. This means that non-magnetic atoms can introduce magnetism in Bi₂Se₃.

The total magnetic moments (M_{tot}) and single X atom moments (M_{X}) are listed in Table 1. The ferromagnetism mainly comes from the doped atoms, and the doped atoms also have an effect on the surrounding atoms. The magnetic moments of BBi, BSe2, CBi, CSe1, CSe2, Cgap, NSe2 and Ngap are 0.978 μB, 1.416 μB, 0.410 μB, 0.649 μB, 0.980 μB, 0.673 μB, 0.094 μB and 0.794 μB, respectively. As illustrated in our results, the magnetic moments

are generally reasonable and closer to the experimental data. Specifically, the bond lengths decrease and the covalent bonds become stronger with X atoms doping. There are more charges transferring to the dopant X from adjacent atoms and occupying the empty 2p orbitals of the dopant. The 2p orbital of the dopant atoms become less localized or even delocalized. The bond lengths and transferred charges are different when X dopes different sites. The magnetic moments' variation accompanies the change of charges. Thus, the magnetic moments and the bond lengths vary for different sites in this case. It is noted the magnetic moment can be introduced when C atoms are doped at each position, suggesting that C is the most effective dopant. In addition, the X atom doping at the Se2 site always introduces the magnetic moment, and the magnetic moment is larger than that of the Se1 site. In the experiment, it is difficult to control the doping element to replace the Se2 site definitely, so the best way to introduce magnetism is through C atom doping.

3.2. Electronic Structure of C Doping Bi_2Se_3

Next, we focus on the electronic structure of C doping Bi_2Se_3 because C doping can introduce magnetism at each doping position. The valence band maximum (VBM) of the perfect Bi_2Se_3 is dominated by the p states of Se1 and Se2, whereas the conduction band minimum originates (CBM) from Bi-6p without SOC. Due to the effect of spin orbit coupling, the VBM mainly derives from the p states of the 6p electrons of the Bi atom; the 4p electrons of the Se atom shift from VBM to CBM. The energy band reversed at the Γ point with SOC, as shown in Figure 2. Figure 3 is the band structures of C atoms doping Bi_2Se_3 with the SOC functional. The Fermi level is set at the energy zero point and the band structure ($-1\sim 1$ eV) close to the Fermi level is given.

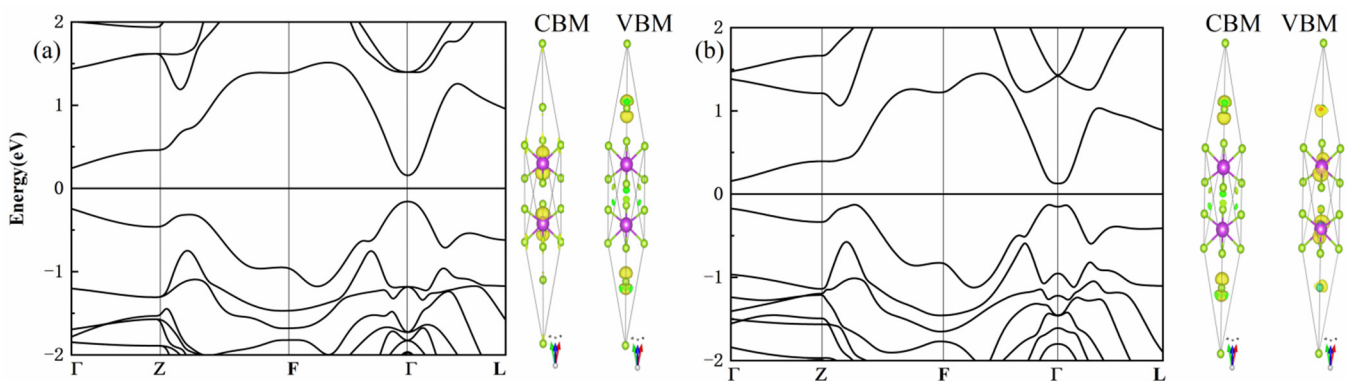


Figure 2. Band structure and partial charge of Bi_2Se_3 : (a) GGA and (b) SOC.

The impurity energy band mainly originating from the doped atom is localized near the Fermi level. This shows that the energy band of Bi_2Se_3 can be regulated by non-magnetic atoms doping. The impurity states mixing with the time-reversal paired states resulted in the substantial modifications of the electronic structure. Even when the contribution of dopants in the bands is very weak, the dopants have a very large impact on the band gap, band curvature and Fermi level, varying wildly depending on the position of the dopant. To make the impurity states more obvious, the contribution of the C atoms was magnified 10 times.

The C substitution for Se created a hole carrier because Bi atoms can accommodate three electrons but there are not enough electrons for the C atom to bond with the surrounding Bi atoms. Thus, in Figure 3b,c, the impurity band near the Fermi level mainly derives from the hole carrier. Moreover, because Se2 atoms are in the center of the QL and strongly localized, there is more than one impurity band between the valence band and the conduction band. In Figure 3a,d, the Fermi level moves up into the conduction band. The Fermi level undergoes an evident shift in energy, presenting somewhat metallic behavior, and the insulation properties are damaged. In C_{gap} , the impurity bands appear in the gap to accommodate the introduced unpaired electrons. The energy degeneracy is

more obvious because the van der Waals force is weaker than the covalent bond. Similar to pure Bi_2Se_3 , the energy band reversed at the Γ point, indicating that the doped system still maintains topological properties. The conduction band is contributed by Bi-p states. The valence band is derived from the Se-p states and the C-2p orbital. The bottom of the conduction band at the Γ point still mainly comes from the p-electron contribution of the Se atom, and the valence band top comes from the p-electron contribution of the Bi atom.

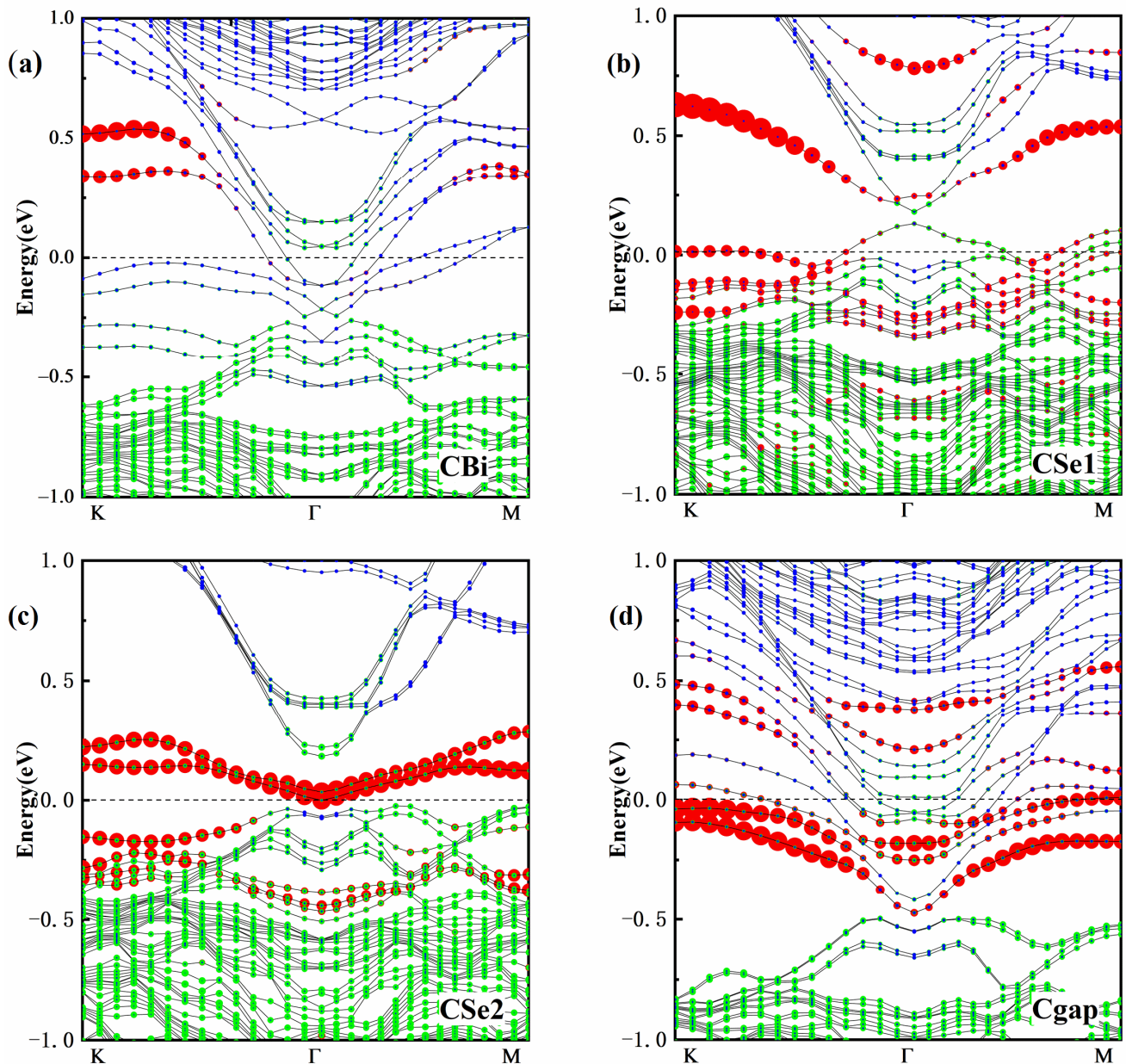


Figure 3. Band structure of C doping Bi_2Se_3 : (a) C doping at Bi site, (b) C doping at Se1 site, (c) C doping at Se2 site, and (d) C doping at gap site. The black line is the total band, the red point is the contribution from C atom, the green point is the contribution from Se atom and the blue point is the contribution from Bi atom.

Figure 4 shows the total density of states (DOS) and partial density of states (PDOS) after doping. To make the impurity states more obvious, the intensity of the integral C-2p states was 30 times larger. The narrow highly localized impurity bands exhibiting an obvious spin split around the Fermi level. The spin-up and spin-down densities of states are offset and asymmetrical, indicating the appearance of magnetism. In CSe1 and CSe2,

it is obvious that for the spin-up channel there is an energy gap around the Fermi level while the minority spin-down bands cross the Fermi level. The substituted structures are half-metallic ferromagnetic. This is different from the CBi and Cgap, where the majority spin channel is metallic.

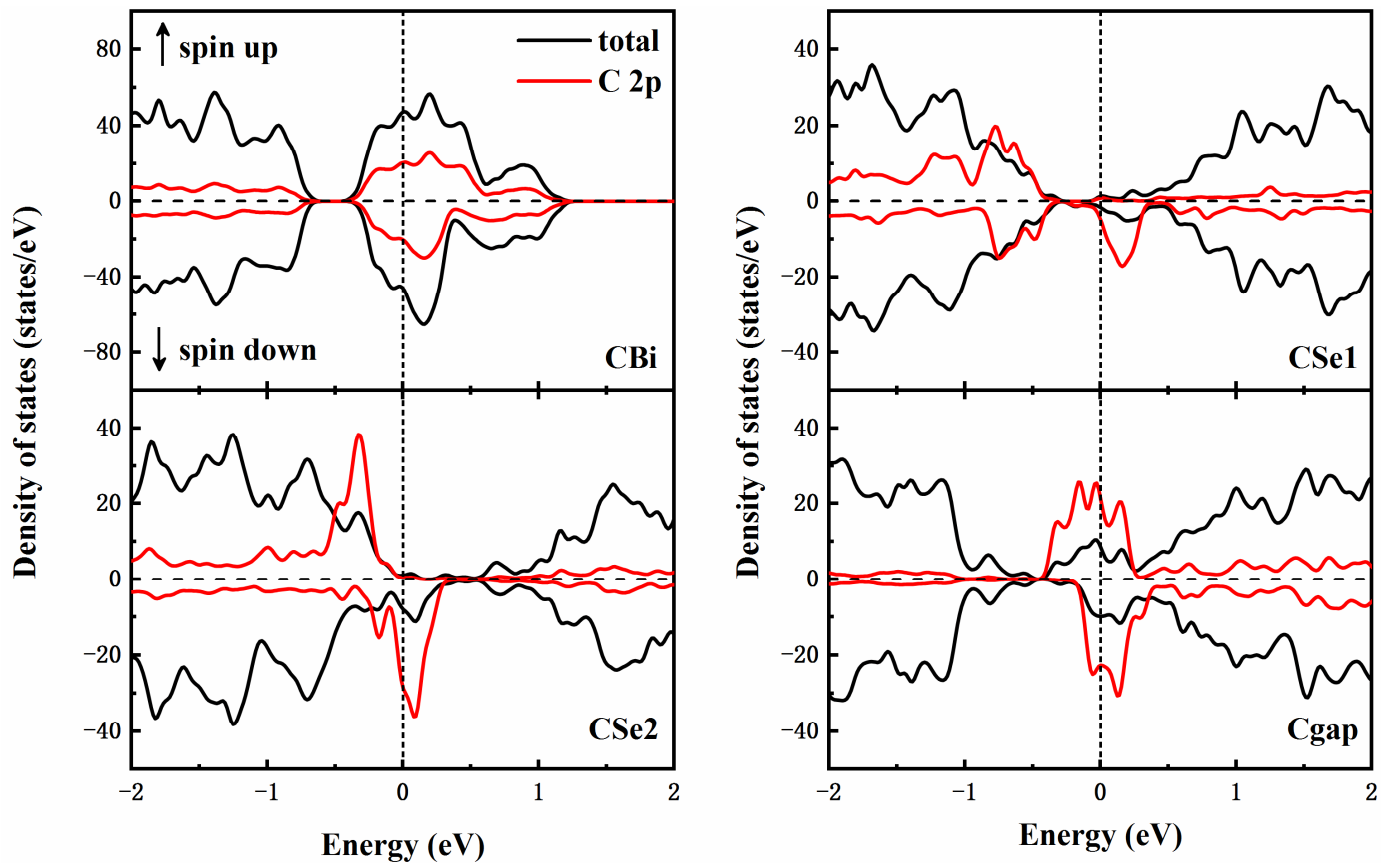


Figure 4. The total DOS and PDOS of C doping Bi_2Se_3 .

In order to verify the magnetism of C-doped samples, single crystal samples were prepared and magnetization versus applied magnetic field curves for $\text{C}_x\text{Bi}_2\text{Se}_3$ was measured at 15 K. The estimated diamagnetic susceptibility was about $\chi_0 = -8.22 \times 10^{-5}$ emu/mol, which is close to that of pure Bi_2Se_3 . Similar diamagnetic signals are also obvious in the C-doped samples, as shown in Figure 5a. After subtraction of the paramagnetic signals from the total signals, hysteresis loops were extracted from the experimental data [35]. As can be seen in Figure 5b, the magnetic saturation moment per C atom was 0.0235~0.0375 μ_B , as listed in Table 2. In spite of supposing a very low amount of C atom in Bi_2Se_3 , it is also possible to measure the coercivity H_c (shown in Table 2). As the concentration of C increases, the M_{Smol} values increase obviously. The coercive field H_c varies from 112 Oe to 232 Oe, nearly invariant of the C concentration. It is noted that the remnant magnetization M_r increases with the C concentration. It can be supposed that ferromagnetism is closely related to C concentration, based on the rising tendency of M_{Smol} and M_r . The experimental magnetic moment of $\text{C}_x\text{Bi}_2\text{Se}_3$ is considerably smaller than the expected atomic moments (shown in Table 1). This may be due to the uneven doping during the preparation process, as only a small part of C enters the lattice. There are clear hysteresis loops at 15 K, which indicates the existence of a ferromagnetic state in $\text{C}_x\text{Bi}_2\text{Se}_3$.

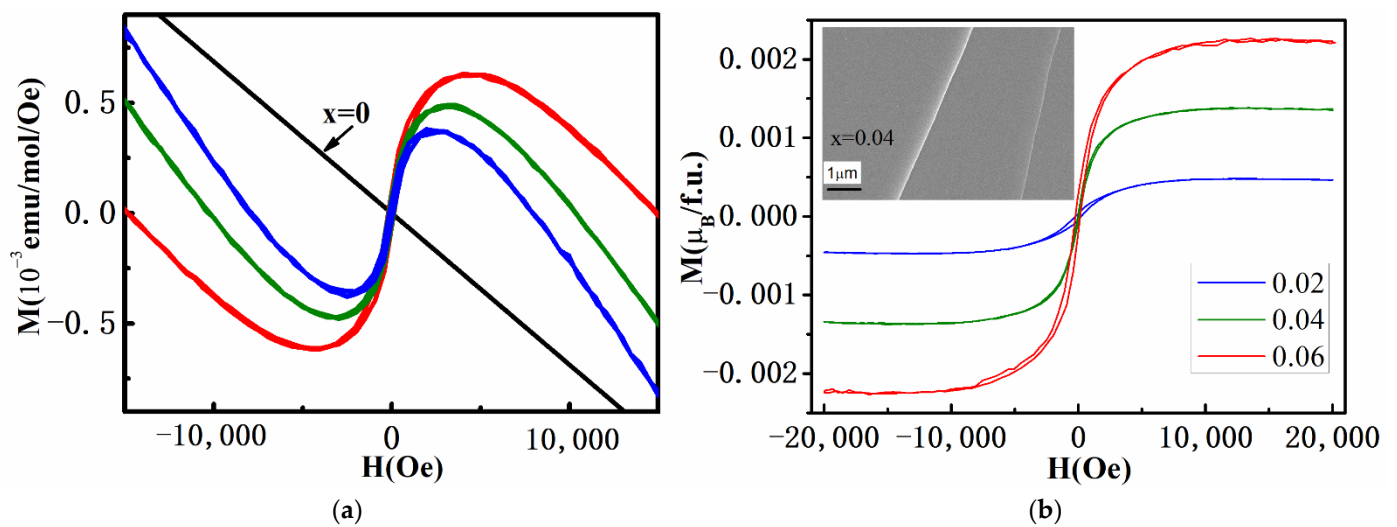


Figure 5. (a) Magnetization versus applied magnetic field for $C_x\text{Bi}_2\text{Se}_3$ measured at 15 K. (b) The magnetic hysteresis loops after subtracting the diamagnetic signals. There is obvious magnetic hysteresis in all doped samples. Inset: FESEM images of $C_{0.06}\text{Bi}_2\text{Se}_3$ crystal.

Table 2. Lists of remnant magnetization, saturation magnetization and coercivity for $C_x\text{Bi}_2\text{Se}_3$.

x	Saturation Magnetization M_{Smol}		Remanent Magnetization M_r [$\mu\text{B}/\text{f.u.}$]	Coercivity H_c (Oe)
	[$\mu\text{B}/\text{f.u.}$]	[$\mu\text{B}/C_{\text{atom}}$]		
0.02	4.71×10^{-4}	0.0235	7.85×10^{-5}	227
0.04	1.37×10^{-3}	0.034	2.1×10^{-4}	112
0.06	2.25×10^{-3}	0.0375	7.5×10^{-4}	232

4. Conclusions

In the present work, the electrical and magnetic properties of the C-doped Bi_2Se_3 topological insulator were discussed. The Fermi level moves up into the conduction band in C_{Bi} and C_{gap} and the insulation properties of the Bi_2Se_3 system are damaged. In CSe1 and CSe2, the substituted structures are half-metallic ferromagnetic. Similar to the transition metals doping, the X atom doping Bi_2Se_3 can induce magnetic moments. It was proved that C is the most effective dopant to induce the magnetism ground states. The remnant magnetization M_r increases with the C concentration. The experiment confirmed the existence of ferromagnetic state in $C_x\text{Bi}_2\text{Se}_3$. The introduction of magnetism by doping with non-magnetic elements can promote the application of topological insulators in spintronic devices.

Author Contributions: Data curation, D.W., L.-G.L. and M.Z.; Formal analysis, L.-G.L., C.-E.H.; Investigation, C.-E.H., X.-R.C.; Methodology, D.W., M.Z. and X.-R.C.; Resources, M.Z.; Writing—original draft, D.W. All authors have read and agreed to the published version of the manuscript.

Funding: This research was funded by National Natural Science Foundation of China (grant Nos. 11804281, 12074274) and the NSAF (grant No. U1830101).

Conflicts of Interest: The authors declare no conflict of interest.

References

- Zhang, W.; Yu, R.; Zhang, H.J.; Dai, X.; Fang, Z. First-principles studies of the three-dimensional strong topological insulators Bi_2Te_3 , Bi_2Se_3 and Sb_2Te_3 . *New J. Phys.* **2010**, *12*, 65013. [[CrossRef](#)]
- Xue, L.; Zhou, P.; Zhang, C.X.; He, C.Y.; Hao, G.L.; Sun, L.Z.; Zhong, J.X. First-principles study of native point defects in Bi_2Se_3 . *AIP Adv.* **2013**, *3*, 52105. [[CrossRef](#)]

3. Qi, X.L.; Li, R.D.; Zang, J.D.; Zhang, S.C. Inducing a Magnetic Monopole with Topological Surface States. *Science* **2009**, *323*, 1184–1187. [[CrossRef](#)] [[PubMed](#)]
4. Zhang, H.J.; Liu, C.X.; Qi, X.L.; Dai, X.; Fang, Z.; Zhang, S.C. Topological insulators in Bi_2Se_3 , Bi_2Te_3 and Sb_2Te_3 with a single Dirac cone on the surface. *Nat. Phys.* **2009**, *5*, 438–442. [[CrossRef](#)]
5. Hsieh, D.; Xia, Y.; Qian, D.; Wray, L.; Dil, J.H.; Meier, F.; Osterwalder, J.; Patthey, L.; Checkelsky, J.G.; Ong, N.P. A tunable topological insulator in the spin helical Dirac transport regime. *Nature* **2009**, *460*, 1101–1105. [[CrossRef](#)] [[PubMed](#)]
6. Chen, J.; Qin, H.J.; Yang, F.; Liu, J.; Guan, T.; Qu, F.M.; Zhang, G.H.; Shi, J.R.; Xie, X.C.; Yang, C.L. Gate-voltage control of chemical potential and weak antilocalization in BiSe. *Phys. Rev. Lett.* **2010**, *105*, 176602. [[CrossRef](#)]
7. Lian, R.; Zhang, J.M.; Yang, Y.; Xu, G.; Huang, Z. Cr doped topological insulator Bi_2Se_3 under external electric field: A first-principle study. *J. Phys. Conf. Ser.* **2017**, *864*, 012039. [[CrossRef](#)]
8. Liu, Q.; Liu, C.X.; Xu, C.; Qi, X.L.; Zhang, S.C. Magnetic Impurities on the Surface of a Topological Insulator. *Phys. Rev. Lett.* **2010**, *102*, 156603. [[CrossRef](#)]
9. Wray, L.A.; Xu, S.Y.; Xia, Y.Q.; Hsieh, D.; Fedorov, A.V.; Hor, Y.S.; Cava, R.J.; Bansil, A.; Lin, H.; Hasan, M.Z. A topological insulator surface under strong Coulomb, magnetic and disorder perturbations. *Nat. Phys.* **2011**, *7*, 32–37. [[CrossRef](#)]
10. Chen, Y.L.; Chu, J.H.; Analytis, J.G.; Liu, Z.K.; Igarashi, K.; Kuo, H.H.; Qi, X.L.; Mo, S.K.; Moore, R.G.; Lu, D.H. Massive Dirac Fermion on the Surface of a Magnetically Doped Topological Insulator. *Science* **2010**, *329*, 659–662. [[CrossRef](#)]
11. Yu, R.; Zhang, W.; Zhang, H.J.; Zhang, S.C.; Dai, X.; Fang, Z. Quantized Anomalous Hall Effect in Magnetic Topological Insulators. *Science* **2010**, *329*, 61–64. [[CrossRef](#)] [[PubMed](#)]
12. Chang, C.Z.; Zhang, J.; Feng, X.; Shen, J.; Zhang, Z.; Guo, M.; Li, K.; Ou, Y.; Wei, P.; Wang, L. Experimental Observation of the Quantum Anomalous Hall Effect in a Magnetic Topological Insulator. *Science* **2013**, *340*, 167–170. [[CrossRef](#)] [[PubMed](#)]
13. Niu, C.; Dai, Y.; Zhang, Z.; Ma, Y.; Huang, B. Ferromagnetism and manipulation of topological surface states in Bi_2Se_3 family by 2p light elements. *Appl. Phys. Lett.* **2012**, *100*, 194. [[CrossRef](#)]
14. Hou, Y.; Wu, R. Magnetizing topological surface states of Bi_2Se_3 with a CrI_3 monolayer. *Sci. Adv.* **2018**, *1874*, 1802.
15. Koirala, N.; Brahlek, M.; Salehi, M.; Wu, L.; Dai, J.; Waugh, J.; Nummy, T.; Han, M.G.; Moon, J.; Zhu, Y. Record Surface State Mobility and Quantum Hall Effect in Topological Insulator Thin Films via Interface Engineering. *Nano. Lett.* **2015**, *15*, 8245–8249. [[CrossRef](#)]
16. Katmis, F.; Lauter, V.; Nogueira, F.S.; Assaf, B.A.; Jamer, M.E.; Wei, P.; Satpati, B.; Freeland, J.W.; Eremin, I.; Heiman, D. A high-temperature ferromagnetic topological insulating phase by proximity coupling. *Nature* **2016**, *533*, 513–516. [[CrossRef](#)]
17. Zhang, J.; Zhao, K.; Yang, X.S.; Zhao, Y. Preparation and Magnetic Properties for $\text{FeSe}_x/\text{Bi}_2\text{Se}_3$ Bilayer Films on Silicon Substrates by RF Magnetron Sputtering. *Funct. Mater. Lett.* **2019**, *12*, 1950018. [[CrossRef](#)]
18. Yang, Q.I.; Dolev, M.; Zhang, L.; Zhao, J.; Fried, A.D.; Schemm, E.; Liu, M.; Palevski, A.; Marshall, A.F.; Risbud, S.H. Emerging Weak Localization Effects on Topological Insulator-Insulating Ferromagnet (Bi_2Se_3 -EuS) Interface. *Phys. Rev. B* **2013**, *88*, 081407.1–081407.4. [[CrossRef](#)]
19. Lee, Y.F.; Kumar, R.; Hunte, F.; Narayan, J.; Schwartz, J. Microstructure and transport properties of epitaxial topological insulator Bi_2Se_3 thin films grown on MgO (100), Cr_2O_3 (0001), and Al_2O_3 (0001) templates. *J. Appl. Phys.* **2015**, *118*, 1057–1110. [[CrossRef](#)]
20. Matetskiy, A.V.; Kibirev, I.A.; Hirahara, T.; Hasegawa, S.; Zotov, A.V.; Saranin, A.A. Direct observation of a gap opening in topological interface states of $\text{MnSe}/\text{Bi}_2\text{Se}_3$ heterostructure. *Appl. Phys. Lett.* **2015**, *7*, 3045. [[CrossRef](#)]
21. Zhu, S.; Meng, D.; Liang, G.; Shi, G.; Wu, K. Proximity-induced magnetism and an anomalous Hall effect in $\text{Bi}_2\text{Se}_3/\text{LaCoO}_3$: A topological insulator/ferromagnetic insulator thin film heterostructure. *Nanoscale* **2018**, *10*, 21. [[CrossRef](#)] [[PubMed](#)]
22. Chang, S.J.; Chuang, P.Y.; Chong, C.W.; Chen, Y.J.; Huang, J.C.; Chen, P.W.; Tseng, Y.C. Heterostructured ferromagnet–topological insulator with dual-phase magnetic properties. *RSC Adv.* **2018**, *8*, 7785–7791. [[CrossRef](#)] [[PubMed](#)]
23. Zhang, H.; Li, H.; Wang, H.; Cheng, G.; Wang, J. Linear positive and negative magnetoresistance in topological insulator Bi_2Se_3 flakes. *Appl. Phys. Lett.* **2018**, *113*, 113503. [[CrossRef](#)]
24. Collins-Mcintyre, L.J.; Harrison, S.E.; Schönherr, P.; Steinke, N.J.; Hesjedal, T. Magnetic ordering in Cr-doped Bi_2Se_3 thin films. *EPL (Europhys. Lett.)* **2014**, *107*, 57009. [[CrossRef](#)]
25. Aramberri, H.; Mufioz, M.C. Gap and spin texture engineering of Dirac topological states at the Cr- Bi_2Se_3 interface. *Phys. Rev. B* **2016**, *93*, 245401.1–245401.7. [[CrossRef](#)]
26. Yilmaz, T.; Hines, W.; Sun, F.C.; Pletikosić, I.; Budnick, J.; Valla, T.; Sinkovic, B. Distinct effects of Cr bulk doping and surface deposition on the chemical environment and electronic structure of the topological insulator Bi_2Se_3 . *Appl. Surf. Sci.* **2017**, *407*, 371–378. [[CrossRef](#)]
27. Tung, Y.; Chong, C.W.; Liao, C.W.; Chang, C.H.; Huang, S.Y.; Chuang, P.Y.; Lee, M.K.; Cheng, C.M.; Li, Y.C.; Liu, C.P. Tuning the transport and magnetism in a Cr- Bi_2Se_3 topological insulator by Sb doping. *RSC Adv.* **2017**, *7*, 47789–47795. [[CrossRef](#)]
28. Choi, J.H.; Lee, W.; Kim, B.S.; Choi, S.; Cho, S. Mn-doped V_2VI_3 semiconductors: Single crystal growth and magnetic properties. *J. Appl. Phys.* **2005**, *97*, 495. [[CrossRef](#)]
29. Wei, Z.; Lv, L.; Zhang, M.; Yang, X.; Zhao, Y. Tuning of Electrical and Magnetic Transport Properties in Bi_2Se_3 Topological Insulator Crystals Doped with Mn. *J. Supercond. Nov. Magn.* **2015**, *28*, 2083–2088. [[CrossRef](#)]
30. Choi, Y.H.; Jo, N.H.; Lee, K.J.; Lee, H.W.; Jo, Y.H.; Kajino, J.; Takabatake, T.; Ko, K.T.; Park, J.H.; Jung, M.H. Simple tuning of carrier type in topological insulator Bi_2Se_3 by Mn doping. *Appl. Phys. Lett.* **2012**, *101*, 152103. [[CrossRef](#)]

31. Choi, J.; Lee, H.W.; Kim, B.S.; Park, H.; Choi, S.; Hong, S.C.; Cho, S. Magnetic and transport properties of Mn-doped Bi₂Se₃ and Sb₂Se₃. *J. Magn. Magn. Mater.* **2006**, *304*, 164–166. [[CrossRef](#)]
32. Von Bardeleben, H.J.; Cantin, L.; Zhang, D.M.; Richardella, A.; Rench, D.W.; Samarth, N.; Borchers, J.A. Ferromagnetism in Bi₂Se₃: Mn epitaxial layers. *Phys. Rev. B* **2013**, *88*, 1336–1340. [[CrossRef](#)]
33. Collins-Mcintyre, L.J.; Watson, M.D.; Baker, A.A.; Zhang, S.L.; Coldea, A.I.; Harrison, S.E.; Pushp, A.; Kellock, A.J.; Parkin, S.S.P.; Van, G. X-ray magnetic spectroscopy of MBE-grown Mn-doped Bi₂Se₃ thin films. *AIP Adv.* **2014**, *4*, 3045. [[CrossRef](#)]
34. Savehenko, D.; Tarasenko, R.; Valiska, M.; Kopecek, J.; Fekete, L. Local moment formation and magnetic coupling of Mn dopants in Bi₂Se₃: A low-temperature ferromagnetic resonance study. *Physica B* **2018**, *536*, 604–613. [[CrossRef](#)]
35. Li, H.; Song, Y.R.; Yao, M.; Zhu, F.F. Carrier density dependence of the magnetic properties in iron-doped Bi₂Se₃ topological insulator. *J. Appl. Phys.* **2013**, *113*, 043926. [[CrossRef](#)]
36. Wei, X.Y.; Zhang, J.Y.; Zhao, B.; Zhu, Y.; Yang, Z.Q. Ferromagnetism in Fe-doped Bi₂Se₃ topological insulators with Se vacancies. *Phys. Lett. A* **2015**, *379*, 417–420. [[CrossRef](#)]
37. Salman, Z.; Pomjakushina, E.; Pomjakushin, V.; Kanigel, A.; Chashka, K.; Conder, K.; Morenzoni, E.; Prokscha, T.; Sedlak, K.; Suter, A. The Nature of Magnetic Ordering in Magnetically Doped Topological Insulator Bi_{2-x}Fe_xSe₃. *Mater. Sci.* **2012**, *1203*, 4850.
38. Yang, H.; Liu, L.G.; Zhang, M.; Yang, X.S. Growth and magnetic properties of Ni-doped Bi₂Se₃ topological insulator crystals. *Solid State Commun.* **2016**, *241*, 26–31. [[CrossRef](#)]
39. Niu, W.; Du, K.; Wang, S.B.; Zhang, M.H.; Gao, M.; Chen, Y.D.; Liu, H.; Zhou, W.; Song, F.Q.; Wang, P. Intrinsic ferromagnetism and quantum transport transition in individual Fe-doped Bi₂Se₃ topological insulator nanowires. *Nanoscale* **2017**, *10*, 1039. [[CrossRef](#)]
40. Zhang, M.; Lv, L.; Wei, Z.T.; Yang, X.S.; Zhao, Y. Ferromagnetism on a paramagnetic host background in cobalt-doped Bi₂Se₃ topological insulator. *Chin. Phys. B* **2014**, *23*, 579–583.
41. Yang, H.; Liu, L.G.; Zhang, M. Anomalous second ferromagnetic phase transition in Co_{0.08}Bi_{1.92}Se₃ topological insulator. *J. Alloys Compd.* **2016**, *678*, 463–467.
42. Harrison, S.E.; Collins-Mcintyre, L.J.; Zhang, S.L.; Baker, A.A.; Hesjedal, T. Study of Dy-doped Bi₂Te₃: Thin film growth and magnetic properties. *J. Phys. Condens. Matter.* **2015**, *27*, 245602. [[CrossRef](#)] [[PubMed](#)]
43. Kim, J.; Lee, K.; Takabatake, T.; Kim, H.; Kim, M.; Jung, M.H. Corrigendum: Magnetic Transition to Antiferromagnetic Phase in Gadolinium Substituted Topological Insulator Bi₂Te₃. *Sci. Rep.* **2015**, *5*, 10309. [[CrossRef](#)] [[PubMed](#)]
44. Harrison, S.E.; Collins-Mcintyre, L.J.; Zhang, S.L.; Baker, A.A.; Figueroa, A.I.; Kellock, A.J.; Pushp, A.; Chen, Y.L.; Parkin, S.S.P.; Harris, J.S. Study of Ho-doped Bi₂Te₃ topological insulator thin films. *Appl. Phys. Lett.* **2015**, *107*, 146802. [[CrossRef](#)]
45. Oveshnikov, L.N.; Rodionov, Y.I.; Kugel, K.I.; Karateev, I.A.; Aronzon, B. Magnetism of Bi₂Se₃ thin films with Eu-rich flat inclusions. *J. Phys. Condens. Matter.* **2018**, *30*, 44. [[CrossRef](#)]
46. Song, Y.R. Large magnetic moment of gadolinium substituted topological insulator: Bi_{1.98}Gd_{0.02}Se₃. *Appl. Phys. Lett.* **2012**, *100*, 195322. [[CrossRef](#)]
47. Moon, J.; Koirala, N.; Salehi, M.; Zhang, W.; Wu, W.; Oh, S. Solution to the hole-doping problem and tunable quantum Hall effect in Bi₂Se₃ thin films. *Nano Lett.* **2018**, *18*, 820. [[CrossRef](#)]
48. Kuntsevich, A.; Bryzgalov, M.A.; Prudkoglyad, V.A.; Martovitskii, V.P.; Chizhevskii, E.G. Structural distortion behind the nematic superconductivity in Sr_xBi₂Se₃. *New J. Phys.* **2018**, *20*, 10. [[CrossRef](#)]
49. Asaba, T.; Lawson, B.; Tinsman, C.; Chen, L.; Corbae, P.; Li, G.; Qiu, Y.; Hor, Y.; Fu, L.; Li, L. Rotational Symmetry Breaking in a Trigonal Superconductor Nb-doped Bi₂Se₃. *Phys. Rev. X* **2017**, *7*, 1. [[CrossRef](#)]
50. Hor, Y.S.; Checkelsky, J.; Qu, D.; Ong, N.; Cava, R. Superconductivity and non-metallicity induced by doping the topological insulators Bi₂Se₃ and Bi₂Te₃. *J. Phys. Chem. Solids* **2010**, *72*, 572–576. [[CrossRef](#)]
51. Peng, H.; Xiang, H.J.; Wei, S.H.; Li, S.S.; Xia, J.B.; Li, J. Origin and Enhancement of Hole-Induced Ferromagnetism in First-Row d⁰ Semiconductors. *Phys. Rev. Lett.* **2009**, *102*, 017201. [[CrossRef](#)] [[PubMed](#)]
52. Dev, P.; Zhang, P. Unconventional magnetism in semiconductors: Role of localized acceptor states. *Phys. Rev. B* **2010**, *81*, 085207. [[CrossRef](#)]
53. Slipukhina, I.; Mavropoulos, P.; Bliigel, S.; Lezaic, M. Ferromagnetic spin coupling of 2p-impurities in band insulators stabilized by intersite Coulomb interaction: Nitrogen-doped MgO. *Phys. Rev. Lett.* **2011**, *107*, 137203. [[CrossRef](#)] [[PubMed](#)]
54. Chakraborty, B.; Nandi, P.K.; Kawazoe, Y.; Ramaniah, L.M. Room-temperature d⁰ ferromagnetism in carbon-doped Y₂O₃ for spintronic applications: A density functional theory study. *Phys. Rev. B* **2018**, *97*, 18. [[CrossRef](#)]
55. Davis, B.A.; Chakraborty, B.; Kalarikkal, N. Room Temperature Ferromagnetism in Carbon Doped MoO₃ for Spintronic Applications: A DFT Study. *J. Phys. Condens. Matter.* **2016**, *28*, 336001. [[CrossRef](#)]
56. Xin, X.; Guo, C.; Pang, R.; Zhang, M.; Shi, X.; Yang, X.; Zhao, Y. Theoretical and experimental studies of spin polarized carbon doped Bi₂Se₃. *Appl. Phys. Lett.* **2019**, *11*, 042401.1–042401.5. [[CrossRef](#)]
57. Kresse, G.; Hafner, J. Ab initio molecular dynamics for liquid metals. *Phys. Rev. B* **1993**, *48*, 13115–13118. [[CrossRef](#)]
58. Perdew, J.P.; Burke, K.; Ernzerhof, M. Generalized Gradient Approximation Made Simple. *Phys. Rev. Lett.* **1996**, *77*, 3865–3868. [[CrossRef](#)]
59. Blochl, P.E. Projector augmented-wave method. *Phys. Rev. B Condens. Matter.* **1994**, *50*, 17953–17979. [[CrossRef](#)]
60. Nakajima, S. The crystal structure of Bi₂Te_{3-x}Se_x. *J. Phys. Chem. Solids* **1963**, *24*, 479–485. [[CrossRef](#)]